In-situ synchrotron radiation study of the aging response of Ti-6Al-4V alloy with different starting microstructures

B. Callegari[a,b], J. P. Oliveira[c], K. Aristizabal[b], R. S. Coelho[d], P. P. Brito[e], L. Wu[f], N. Schell[g], F. A. Soldera[b], F. Mücklich[b], H. C. Pinto[a,*]

[a]University of São Paulo, São Carlos School of Engineering, Department of Materials Engineering, Av. João Dagnone 1100, 13563-120, São Carlos, Brazil

[b]Saarland University, Department of Materials Science and Engineering, Campus D3.3, 66123 Saarbrücken, Germany

[c]UNIDEMI, Department of Mechanical and Industrial Engineering, NOVA School of Science and Technology, Universidade NOVA de Lisboa, 2829-516 Caparica, Portugal

[d]SENAI CIMATEC, Institute of Innovation for Forming and Joining of Materials, Av. Orlando Gomes 1845, 41650-010 Salvador, Brazil

[e]Pontifical Catholic University of Minas Gerais, Av. Dom José Gaspar 500, 30535-901, Belo Horizonte, Brazil

[f]Brazilian Synchrotron Light Laboratory, Brazilian Center for Research in Energy and Materials, Rua Giuseppe Maximo Scolfaro, 10000, 13083-970, Campinas, Brazil

[g]Institute of Materials Research, Helmholtz-Zentrum Geesthacht, Max-Planck-Str. 1, D-21502, Geesthacht, Germany

*Corresponding author. Postal address: University of São Paulo, São Carlos School of Engineering, Department of Materials Engineering, Av. João Dagnone, 1100, 13563-120, São Carlos, SP, Brazil. E-mail address: haroldo@sc.usp.br. Telephone number: +55 16 33738290.

Highlights

- Enhanced response to aging in microstructures with higher amounts of primary α and β.
- Influence of β distribution and composition on secondary α precipitation.
- Influence of α composition on the precipitation of Ti_3Al.
- α' decomposition with increase in c/a ratio, affecting slip systems' activation.
- Behavior of β phase influenced by elemental partitioning.

Abstract

The aging behavior of a Ti-6Al-4V alloy with different starting microstructures was evaluated by means of synchrotron X-ray diffraction, scanning-transmission electron microscopy and micro-hardness measurements. Initial microstructures were produced by thermal and thermomechanical treatments and comprised different morphologies of α phase (martensitic, lamellar, bimodal and globular), as well as the presence or absence of the β phase. Results show that one or more of the following phenomena can take place during aging and contribute to the hardening of the alloy: β decomposition into fine secondary α laths; transformation of the metastable martensitic α' into the equilibrium α phase; and precipitation of the intermetallic Ti_3Al. The composition and distribution of the β phase was shown to affect the precipitation of secondary α during aging, while the composition of the α phase plays a key role on the formation of Ti_3Al. In situ X-ray diffraction studies of the early stages of aging show the kinetics of the α' → α conversion by the reduction in FWHM of XRD reflections, indicate the contribution to hardening by the increase of the c/a ratio and the consequent limitation of active slip systems and depict the chemical homogenization and decomposition of the β phase.

Keywords: Titanium alloys; Aging; Hardening; Phase transformation; Secondary precipitation; Synchrotron X-ray diffraction.

1. Introduction

Ti-6Al-4V alloy (Ti-64; composition in wt%) is the main representative of α + β alloys, responsible for more than 50% of all titanium alloys' applications [1]. Reasons for its intensive application involve the equilibrium of properties such as strength, ductility, toughness and fatigue properties [2–4]. These properties are consequence of the composition, morphology and ratio of present phases, which come as result of the alloy's response to heat treatments and thermomechanical processing [4]. Treatment temperature, cooling rate and degree and mode of deformation are the main processing parameters, influencing the morphology of the α phase, the formation of martensite, the occurrence of texture and the age hardening potential of the alloy [3].

In titanium alloys, solution treatments produce a relatively high amount of β phase, and this condition can be entirely or partially maintained upon quenching. The subsequent hardening and strength increase attained after aging comes as consequence of the decomposition of this metastable β phase and of any martensitic phase that might form during quenching into dispersed phases [5,6]. Morita et al. attribute the strengthening of Ti-6Al-4V alloy during aging after quenching to the precipitation of a refined α phase from the retained β phase [7]. Stephen et al. state that water quenching after solution

treatment provides more degrees of freedom for microstructure and mechanical properties optimization during aging than air or furnace cooling because the water quenched microstructure can consist of a variety of metastable phases, e.g. α', α" and β, which have good response to aging treatments [8]. Hardening of Ti-6Al-4V alloy due to martensite decomposition was investigated by Qazi et al. [9] and by Gil Mur, Rodríguez and Planell [10]. On the other hand, Pederson states that the primary α phase responds better to aging by the precipitation of intermetallic phase Ti_3Al (α_2) due to its enrichment in aluminum and oxygen, which promote the formation of this phase, in comparison with secondary α phase, that precipitates directly from the β phase upon cooling, lean in these said elements [11].

The vast majority of works related to the aging response of Ti-6Al-4V alloys focuses on the effects of solution treatment and aging on the mechanical properties of the alloy. In the work of Venkatesh et al., water quenching after solution treatment followed by aging has led to higher yield strength and ultimate tensile strength, and lower ductility when compared to air cooling + aging [12]. Hémery and Villechaise evaluated the effect of aging on the plastic deformation of Ti-6Al-4V alloy and found that short range ordering and precipitation of Ti_3Al affects the activation of slip systems: before aging, basal systems are activated first and prismatic systems are subsequently activated, whereas after aging both systems are activated simultaneously [13]. The precipitation of Ti_3Al has been acknowledged to increase the alloy's strength and decrease its ductility [14].

Very few studies focused on tracking the alloy's microstructural behavior under aging treatments exist in the literature. Carreon et al. have studied the response of the microstructure of a Ti-64 alloy to isothermal treatments using thermoelectric methods and hardness measurements, and have attributed the behavior of the alloy to the precipitation of Ti_3Al particles [15]. El-Hadad et al. studied microstructural changes in a solution-treated Ti-6Al-4V alloy after aging at 550°C for 6 h and have observed very few precipitates and no significant hardness evolution in the aged samples, indicating that this aging condition is not enough to induce any relevant microstructural changes in the alloy [16]. Ji et al. have applied thermodynamic simulations to the Ti-6Al-4V alloy and have proposed that, depending on the temperature range in which the isothermal treatment is conducted, different transformation sequences can occur. Between 423 K (~150°C) and 895 K (~620°C), the suggested transformation pathway is $\beta \rightarrow \alpha/\alpha' \rightarrow \alpha + \beta + Ti_3Al$, where the first transformation is diffusionless and the second has a diffusional nature [17].

Given the relevance of Ti-64 alloy for structural applications, the present study aims to understand its microstructural evolution during aging treatments for a better correlation of such evolution with the final properties of the aged alloy in a concise manner. Different thermal and thermomechanical treatments were imposed to the alloy to produce microstructural variability in terms of α phase

morphology and ratio between α and β fractions in order to evaluate the response of each microstructure to subsequent treatments. All conditions underwent aging at 500°C for 24 h and post-aging samples were analyzed by means of high energy X-ray diffraction, transmission electron microscopy and micro-hardness measurements. Shorter aging treatments at 500°C with 8 h of duration were carried out using in situ synchrotron X-ray diffraction for a better understanding of the alloy's response to the isothermal treatment based on their behavior in the initial stages of aging.

2. Materials and methods

2.1. Material

The composition of the Ti-64 alloy (grade 23) used in this work is given in **Table 1**. Contents of heavier elements (Al, V and Fe) were determined by inductively coupled plasma atomic emission spectrometry in an Ametek® SPECTROMAXx analyzer, and amounts of interstitial elements (O, C, N and H) were analyzed using Leco® RO-400, Leco® ONH-836 and Leco® CS-844 analyzers. Its β-*transus* temperature was determined to be of approximately 963°C with a Netzsch® 404 F3 Pegasus differential scanning calorimeter during continuous heating at 20°C/min.

Element	Ti	Al	V	Fe	O	C	N	H
wt%	Bal.	6.03	4.18	0.24	0.14	0.013	0.011	0.006
[Al]eq		7.4		**[Mo]eq**			3.4	

Table 1. Composition of Ti-64 alloy used in this work.

2.2. Tailoring of initial microstructures

The alloy was thermally treated and thermomechanically processed by means of uniaxial compression at 1050°C (β field), 900°C and 700°C (α + β field). Specimens with dimensions of ϕ10 × 15 mm were machined from the as-received bar with their length parallel to the bar's length. To remove any effects of prior processing, specimens initially underwent a homogenization treatment at 1050°C during 30 minutes in an EDG 10P-S furnace with vacuum and argon atmosphere protection followed by water quenching to room temperature. From this condition, compressive deformation was imposed to specimens in a Gleeble® 3800 thermomechanical simulator with strain rate of 10^{-3} s^{-1} up to a compression ratio of 0.5 (true strain = 0.7). Before compression, except for deformation at 1050°C, samples were soaked at the target temperature for 30 minutes. Type-S thermocouples were spot-welded to samples in their mid-length for temperature control, and a conductive silver-graphite paint was applied between specimens' parallel faces and compression anvils to improve thermal contact and lubrication.

Heat-treatments at 900°C and 700°C during 30 minutes followed by water quenching were also done after the initial homogenization at 1050°C. For standardization purposes, each condition was identified based on treatment temperature ("1050C" for 1050°C, "900C" for 900°C and "700C" for 700°C) and type ("HT" for heat treatment and "D" for compression). **Fig. 1** summarizes the processing routes imposed to the alloy.

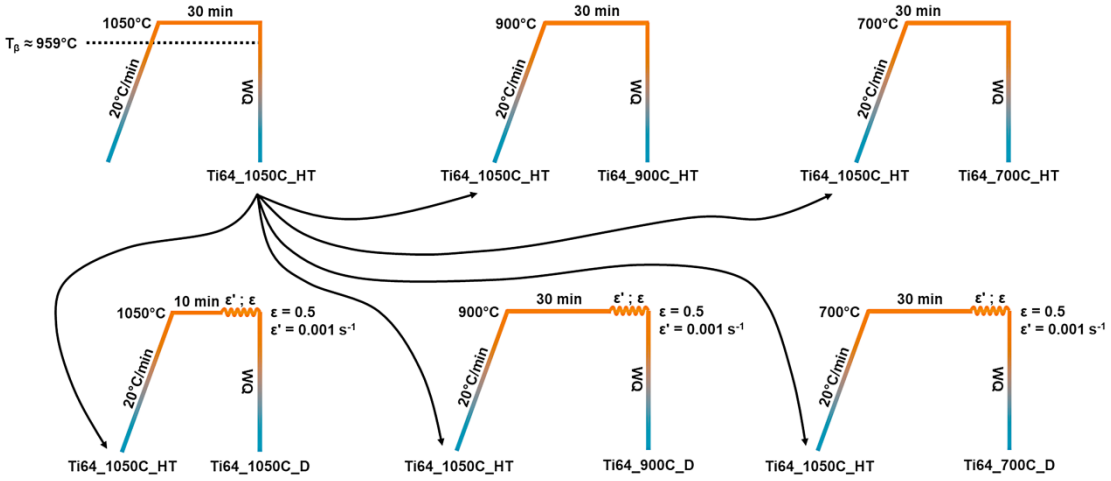

Fig. 1. Schematic representation of thermal and thermomechanical treatments imposed to Ti-64 alloy.

2.3. Microstructural characterization

The alloy was metallographically prepared for scanning electron microscopy (SEM) according to the following procedure: manual grinding on sandpapers with #320, #600 and #1200 grits, automated pre-polishing with a 3-µm diamond suspension and automated polishing using a solution composed by 90 vol% 0.04 µm OP-S and 10 vol% H_2O_2 in a Buehler® EcoMet 250 machine (force: 5N; base rotation: 20 rpm; head rotation: 60 rpm; counter-rotation). SEM analyses were conducted in a FEI® Inspect F50 microscope with field emission gun using secondary (SE) and backscattered electrons (BSE) imaging modes. For the BSE analyses, samples were unetched, and for SE analyses samples were chemically etched with Kroll's etchant (3 mL hydrofluoric acid, 6 mL nitric acid and 91 mL water).

2.4. Aging treatments using synchrotron X-ray diffraction

All conditions were aged at 500°C and analyzed using synchrotron X-ray diffraction. The aging temperature was chosen based on the following criteria: it should be high enough to allow for diffusion but it stands below the *solvus* temperature of Ti_3Al, to allow its precipitation. A simplified verification of the *solvus* temperature was done on ThermoCalc® software using COST 507 database [18] and the

procedure developed by Zhang et al. to describe a pseudo-ternary Ti-Al-V system based on the composition of the multicomponent Ti-64 alloy given in **Table 1** [19]. By this procedure, the obtained *solvus* temperature was of ~548°C. In addition, the chosen temperature should not cause excessive oxidation of the material. Samples with 3 × 4 × 6 mm³ were wire-cut from the previously heat-treated and deformed specimens. In the case of deformed conditions, samples were machined with their length parallel to the compression direction. Aging treatments with holding time of 24 h were done in a Carbolite STF 15/75/450 tube furnace with vacuum level of ~10^{-4} mbar followed by furnace cooling and samples pre- and post-aging were analyzed in the P07B beamline of the PETRA III facility at DESY (Hamburg, Germany). The energy of the beam was 87.1 keV (λ = 0.142 Å). Complete Debye-Scherrer rings were acquired in transmission mode using a Perkin Elmer® XRD 1621 flat panel detector with 200 × 200 μm² pixel size with an exposure time of 0.1 s and 5 frames/image and a spot size of 1 × 1 mm². A standard LaB_6 powder was used for calibration on FIT2D software. The corresponding diffratograms were integrated from the images using an ImageJ software macro.

Shorter aging treatments with holding time of 8 h using in situ synchrotron X-ray diffraction were done in the XTMS experimental station of the XRD1 beamline at the Brazilian Synchrotron Light Laboratory equipped with an adapted Gleeble® 3S50 thermomechanical simulator. The energy of the beam was of 12 keV (λ = 1.033 Å). Temperature control was done using spot-welded K-type thermocouples. The experiment was conducted in reflection mode with a spot size of 1 × 2 mm². Sections of Debye-Scherrer rings were acquired with 60 s of exposure time using a Rayonix® SX165 area detector with pixel size of 39 × 39 μm². Calibration was done using a standard Al_2O_3 powder [20]. Acquired images were processed on Dracon software, a MATLAB® macro developed by the XTMS staff, for the integration of diffractograms.

X-ray diffraction data were analyzed quantitatively using Rietveld refinement on MAUD software [21] for the withdrawal of information such as phase fractions and lattice parameters. Calculation of the full width at half maximum (FWHM) of peaks was done on PeakFit software using a Lorentz + Gauss profile.

2.5. (Scanning) transmission electron microscopy

Samples Ti64_900C_HT, Ti64_900C_D and Ti64_700C_D aged at 500°C during 24 h were selected for transmission (TEM) and scanning-transmission (STEM) electron microscopy analyses. TEM lamellae were prepared by lift-out in a FEI® Helios NanoLab 600 DualBeam microscope. Analyses were

carried out in a FEI® Tecnai G²-F20 transmission electron microscope with field emission gun operated at 200 kV. Indexing of selected area diffraction patterns was done using PTCLab software [22].

2.6. Micro-hardness measurements

The Vickers hardness of samples before and after aging at 500°C for 24 h was measured in a Struers® DuraScan with load of 0.2 kgf. Twenty-five measurements were done with a spacing of 150 μm between each indentation in a 5 × 5 matrix in the center of samples. For the hardness testing, specimens were metallographically prepared as described in **Section 2.3**.

3. Results

3.1. Initial microstructures

Fig. 2 shows the microstructures produced via thermal treatment and thermomechanical processing to compose the initial conditions used for subsequent aging treatments. In some cases, backscattered electrons' signal was used for a better visualization of α and β phases based on chemical contrast. The applied processing pathways achieved all typical microstructures of titanium alloys in terms of α phase morphology, namely martensitic, lamellar, globular and bimodal. Both heat treatment and deformation at 1050°C produced martensitic microstructures. Heat-treatment at 900°C, on the other hand, resulted in coarsening of the α phase, producing a Widmanstätten-like microstructure with a lamellar width of approximately 2 μm, against a width of 0.8 μm in martensitic laths. Hot working at 900°C produced the so-called bimodal microstructure, comprising a coarse globularized α phase formed during deformation (primary α) and colonies of fine laths of α precipitated within the β matrix during rapid cooling (secondary α). With respect to heat treatment at 700°C, a partially martensitic microstructure is seen, with the presence of relatively coarse α lamellae when compared to those seen in Ti64_1050C_HT. Finally, deformation at 700°C yielded a fully globular α microstructure embedded in a β matrix.

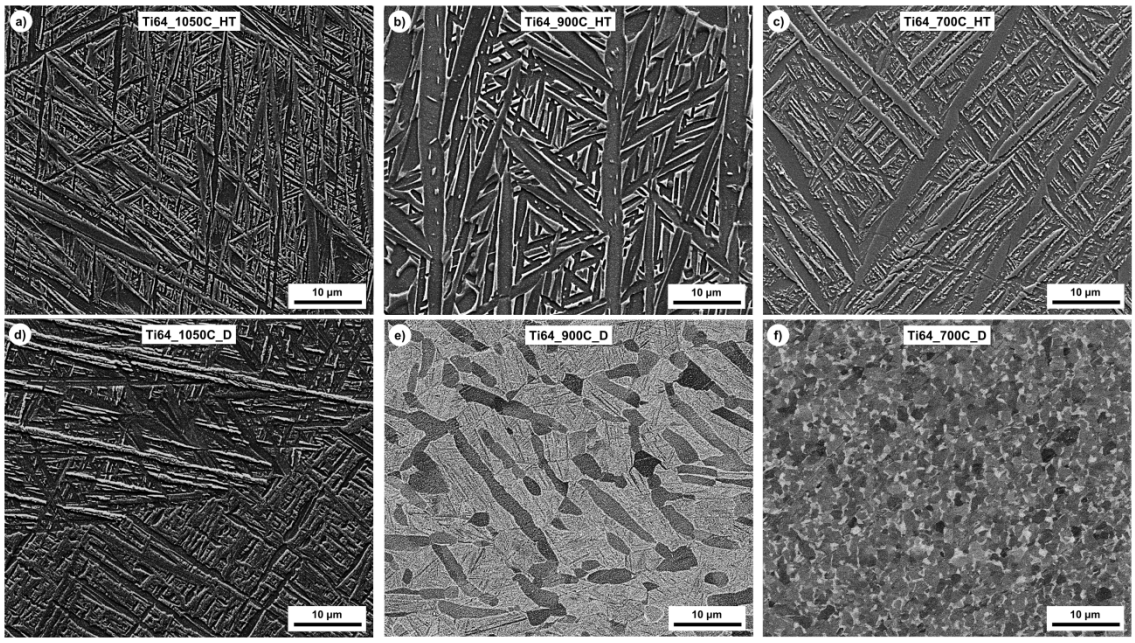

Fig. 2. SEM images of **a)** Ti64_1050C_HT (SE), **b)** Ti64_900C_HT (SE), **c)** Ti64_700C_HT (SE), **d)** Ti64_1050C_D (SE), **e)** Ti64_900C_D (BSE) and **f)** Ti64_700C_D (BSE). In deformed conditions, the compression axis is parallel to the height of images. The α phase is darker and the β phase is brighter.

3.2. Microstructure and hardness evolution

Fig. 3 presents the diffractograms resulting from the complete integration of Debye-Scherrer rings for all conditions before and after aging at 500°C/24 h. The initial diffractogram of Ti64_900C_HT is shown in **Fig. 3g** as a support to identify reflections from α and β phases. No new reflections belonging to phases other than the allotropic ones were seen. The most outstanding difference between non-aged and aged conditions lies on the absence of visible reflections of the β phase after 24 h of aging in all conditions where it was initially present.

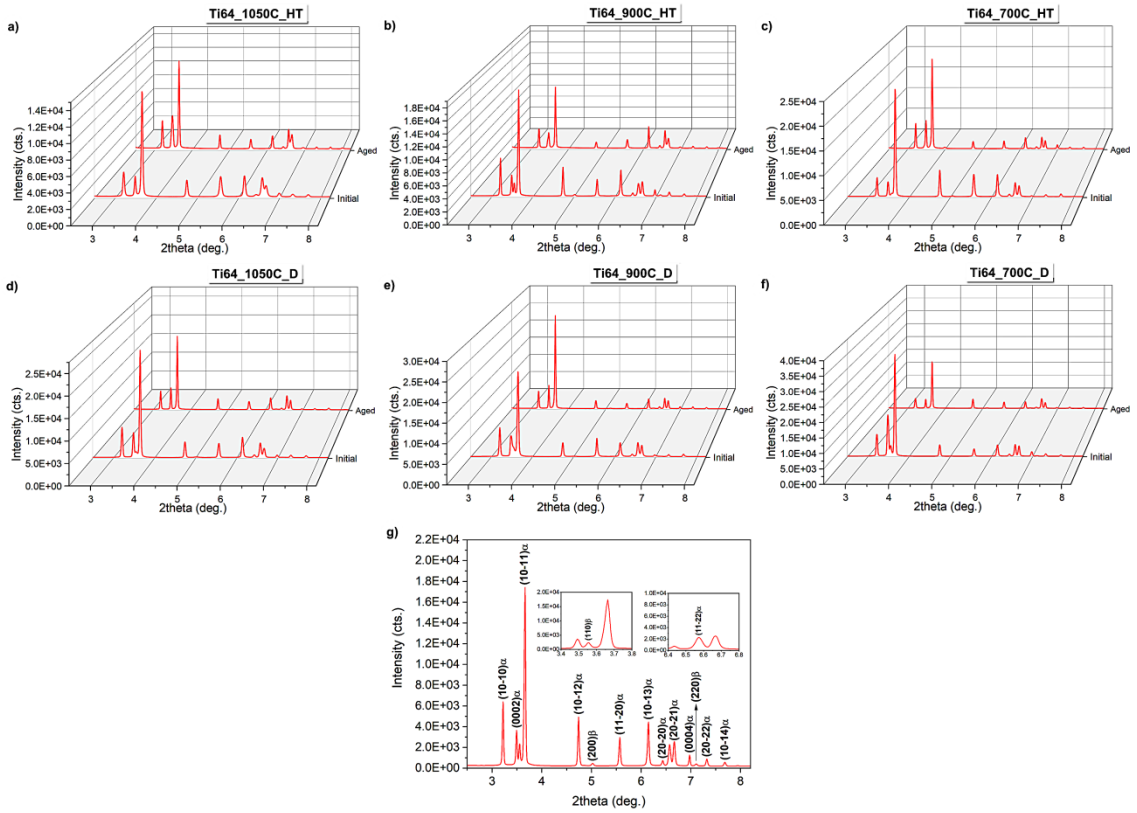

Fig. 3. Integrated diffractograms of initial (pre-aging) and aged conditions: **a)** Ti64_1050C_HT, **b)** Ti64_900C_HT, **c)** Ti64_700C_HT, **d)** Ti64_1050C_D, **e)** Ti64_900C_D and **f)** Ti64_700C_D, with **g)** indication of α and β reflections using the initial diffractogram of Ti64_900C_HT as example.

The initial volume fractions of β phase ($R_{wp} \leq 0.121$) are shown in **Table 2**. It is worth pointing out that Ti64_1050C_D condition contained some remaining metastable β after quenching, differently from Ti64_1050C_HT condition, which has shown a fully martensitic microstructure. As consequence, its hardness was relatively lower, as can be seen in **Fig. 4**. Another contribution to the lower hardness might have its origins on the softening of the alloy caused by dynamic recrystallization of the β phase during deformation [23]. Overall, initial hardness values result from the combination of the amount of the soft β phase and the size and morphology of the α phase.

Condition	Ti64_1050C_HT	Ti64_900C_HT	Ti64_700C_HT
β fraction (%)	-	9.8 ± 0.7	5.5 ± 0.8
Condition	Ti64_1050C_D	Ti64_900C_D	Ti64_700C_D
β fraction (%)	5.5 ± 0.8	8.8 ± 0.5	9.4 ± 0.5

Table 2. Initial volume fractions of the β phase in all conditions of Ti-64 alloy.

During aging, all conditions underwent a hardness increase. It is important to notice that the highest hardness value after aging is presented by Ti64_1050C_HT, which is in agreement with the literature regarding the strength of the alloy with an aged martensitic microstructure [12]. However, results show that the response of the alloy to aging is maximized in microstructures containing a high amount of β and primary α phases. The most significant hardness raises occurred in Ti64_700C_D, Ti64_900C_HT and Ti64_900C_D conditions. This is in agreement with the decomposition of β phase observed in **Fig. 3**, given that these conditions were the ones with the highest initial contents of this phase, whose stabilization upon quenching after solution treatment is useful to enhance the alloy's response to subsequent aging treatments by its decomposition [4]. Thermodynamic simulations as described in **Section 2.4** show that the equilibrium amount of β phase at 500°C is ~2.5 wt%. It is known that, during aging, the alloy tends to reach the equilibrium microstructure for the treatment temperature in terms of phase fractions, and present phases tend to reach their stable chemical composition [4]. Thus, it is reasonable to assume that, in all conditions studied which contained the β phase in their initial microstructure, the amount of β has decreased during aging aiming to achieve thermodynamic stability. Regarding martensitic microstructures, i.e. Ti64_1050C_HT, Ti64_1050C_D and Ti64_700C_HT, the increase in hardness comes as a result of the transformation of the metastable α' into the stable α phase [9,10,12,24]. In the last two conditions, there is the additional effect of decomposition of the remaining metastable β phase.

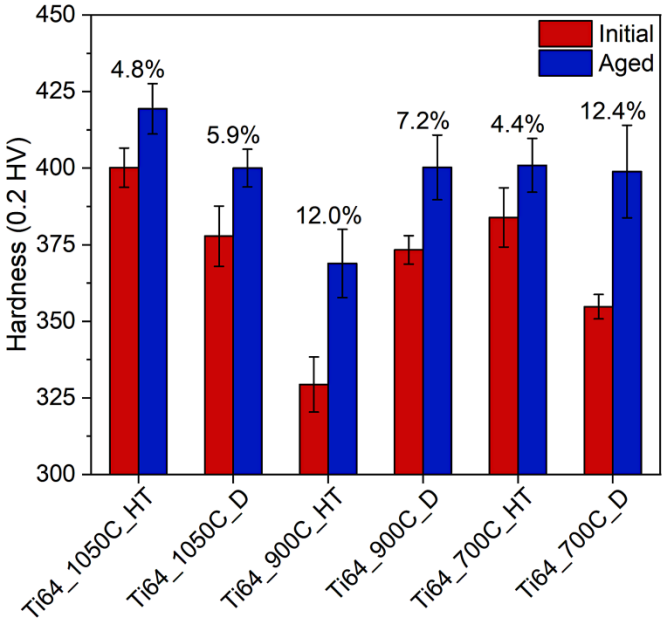

Fig. 4. Hardness evolution of all conditions of Ti-64 alloy after aging at 500°C/24 h with indication of the resulting percent increase.

4. Discussion

4.1. Secondary α precipitation and β decomposition

In order to evaluate microstructural evolution in detail and identify additional hardening mechanisms other than α' and β decomposition, the three conditions with the highest hardness increases mentioned above were analyzed by (S)TEM. **Fig. 5** shows bright field (BF) detail images of the aged microstructures of Ti64_900C_HT, Ti64_900C_D and Ti64_700C_D conditions for 24 h. Overall, no noticeable differences can be seen in comparison with the starting microstructures shown in **Fig. 2**. However, in Ti64_900C_HT condition (**Fig. 5a**), it is possible to observe a β island with extremely refined precipitates between primary α grains.

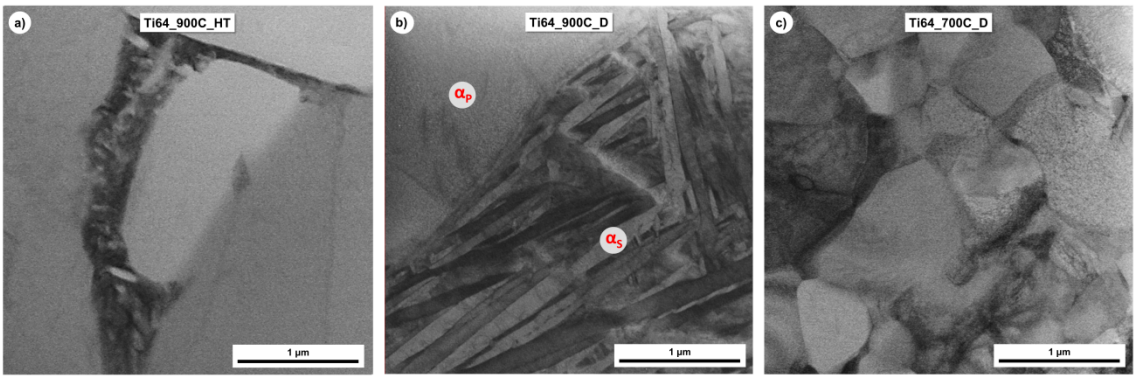

Fig. 5. Bright field image details of the aged microstructures of **a)** Ti64_900C_HT, **b)** Ti64_900C_D, where α_P denotes the primary α phase and α_S, the secondary α phase, and **c)** Ti64_700C_D.

Fig. 6 shows a BF STEM image of Ti64_900C_HT condition after aging during 24 h accompanied by energy dispersive spectroscopy (EDS) maps, which indicate that these refined precipitates are lean in β-stabilizing elements V and Fe and enriched with Ti and Al, therefore consisting of extremely refined secondary α laths. Such features were not observed in the microstructure of Ti64_900C_HT condition before aging. These results show that β decomposition into secondary α occurs during aging, similarly to what has already been observed during annealing of the alloy after hot isostatic pressing [25]. It is important to emphasize that these precipitates were not observed in Ti64_700C_D condition after aging. This difference can be a consequence of the difference in morphology and distribution of the β phase in both conditions, which appears to play a key role, since this phase presents itself continuous along the α laths in the Widmanstätten structure, whereas in the globular structure it is concentrated in triple α boundaries, in a non-uniform manner.

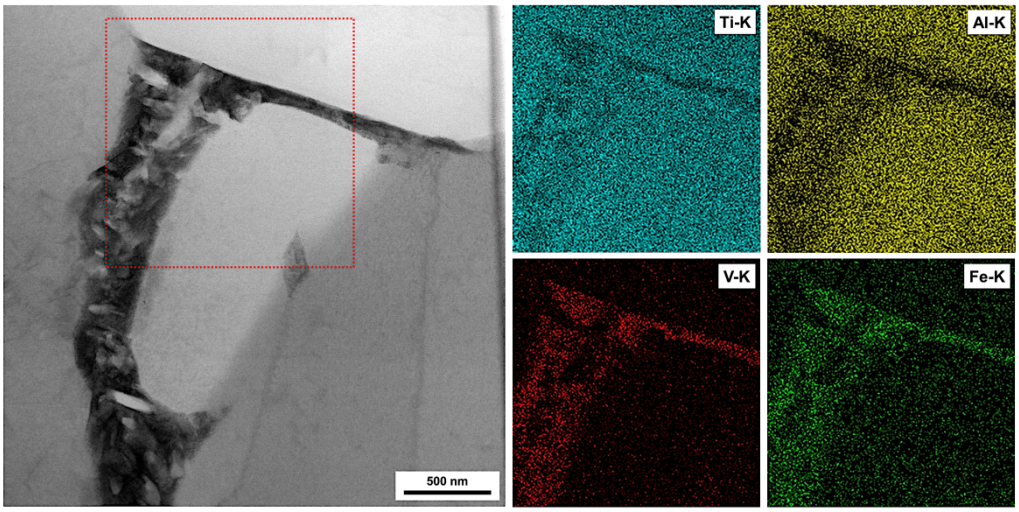

Fig. 6. A bright field STEM image of aged Ti64_900C_HT condition with the EDS maps of Ti, Al, V and Fe of the area delimited by the red square with preserved scale.

Fig. 7 shows a high angle annular dark field (HAADF) image of a secondary α colony in Ti64_900C_D condition. It is possible to notice the presence of the β phase (bright) in the interfaces between adjacent α laths (dark). The qualitative EDS line scan of a region between two adjacent laths shows the enrichment of these regions with β-stabilizing elements V and Fe. As previously discussed, the amount of β decreases towards its equilibrium value during aging. The amount of α increases at the expense of β dissolution. At the end of the aging treatment, extremely thin layers of β remain among α laths.

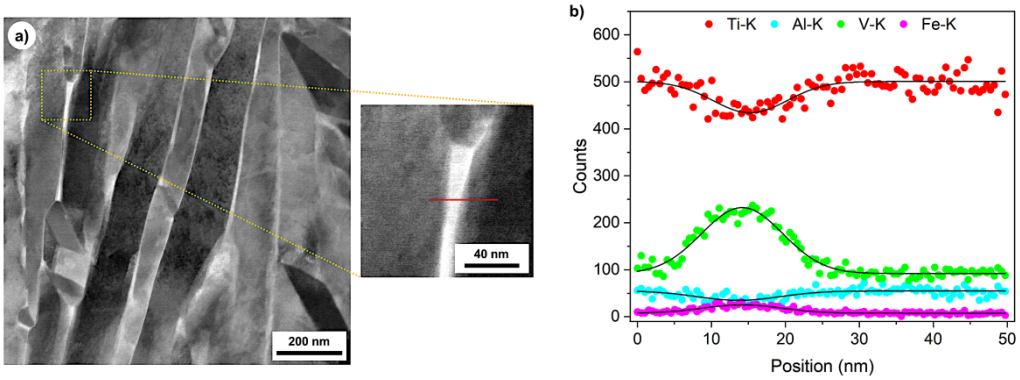

Fig. 7. a) STEM-HAADF image of a secondary α colony in aged Ti64_900C_D condition, with indication of the line scan region, and **b)** the resulting spectra of the line scan.

4.2. Precipitation of Ti_3Al (α_2)

In **Fig. 8** are shown selected area electron diffraction (SAED) patterns of the <1$\bar{1}$01>α zone axis of Ti64_900C_D and Ti64_700C_D conditions after aging. In both cases, the selected area was inside an α grain. With respect to the first, the selected area was inside a primary α grain. In the SAED, in addition

to the α spots belonging to the zone axis, additional spots can be seen. These spots can be attributed to the presence of the intermetallic phase Ti_3Al (α_2). The low signal-to-noise ratio of superlattice reflections in SAED has been previously reported and attributed to the excessively small size of ordered domains [14,26]. Radecka et al. have emphasized that this implicates in a limitation to image these ordered regions using dark field [26]. This also explains the absence of any visible α_2 reflections in the diffractograms shown in **Fig. 3**. Quality dark field TEM images have been acquired in samples aged for significantly longer times, e.g. Ti-6.6wt% Al aged at 825 K during one week [27], Ti-7wt% Al alloy aged for 84 days at 550°C [26] and Ti-64 alloy aged during 5 weeks at 500°C [14], showing ellipsoid-shaped precipitates with their long axis parallel to the c-axis direction. In the early stages of precipitation, these particles present a spherical shape, which evolves to the ellipsoid-like with growth. This morphology had already been observed in earlier studies on Ti-Al alloys [28,29]. After 5 weeks at 500°C, particles with diameters ranging between 5 and 10 nm were observed in the Ti-64 alloy [14]. The precipitation of Ti_3Al obeys the following orientation relationship with α phase: $[\bar{4}223]\alpha \parallel [2\bar{1}\bar{1}\bar{3}]\alpha_2$, $(01\bar{1}0)\alpha \parallel (01\bar{1}0)\alpha_2$ [30].

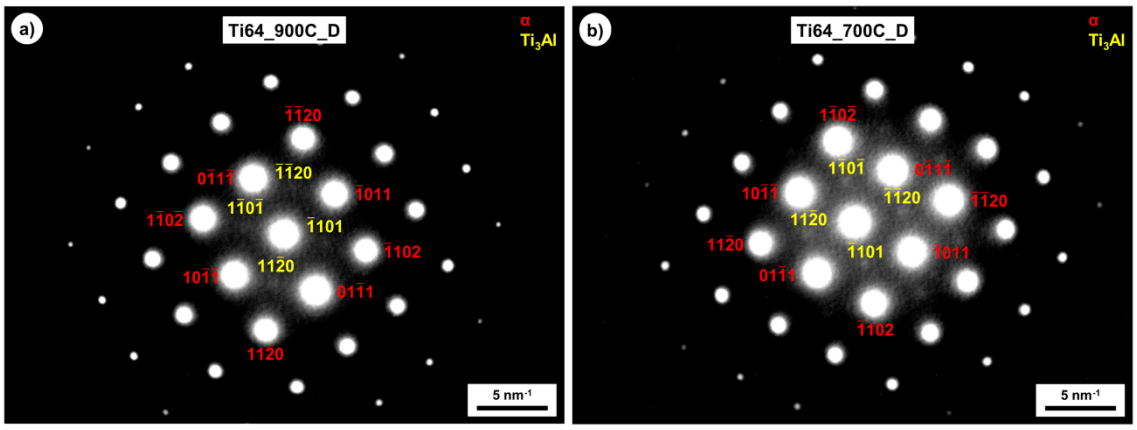

Fig. 8. SAED patterns of the <**1$\bar{1}$01**>α || <**1$\bar{1}$02**>α_2 zone axis of **a)** Ti64_900C_D and **b)** Ti64_700C_D aged conditions with indication of α and Ti_3Al reflections.

This phase is known to precipitate in Ti-64 alloy during long aging treatments at temperatures close to 500°C [26,31]. An aging time of 24 h is regarded as sufficient to promote the formation of α_2 [31]. Such precipitation is attributed to solute partitioning in primary α grains [32]. The β phase is lean in elements such as aluminum and oxygen, which promote the precipitation of coherent Ti_3Al particles and the consequent age hardening. As a result, secondary α lamellae, which form from the β phase upon cooling, do not respond as well as primary α to aging [11]. The precipitation of Ti_3Al is known to increase the tensile strength of Ti-64 alloy, but, on the other hand, it lowers its ductility and fatigue resistance [14,26,32].

It is worth mentioning that these reflections were not seen in SAED patterns of the α phase in the Ti64_900C_HT condition, which shows that the globular α phase produced by thermomechanical treatment is richer in α-stabilizing elements than the α lamellae obtained by annealing. The explanation for this behavior most likely lies in the fact that the imposition of deformation has been shown to significantly enhance diffusive activity in the alloy in comparison with sheer thermal treatment [33]. Furthermore, the total holding time during annealing was of 30 minutes, whereas the thermomechanically processed specimen has undergone an isothermal holding of 30 minutes plus 8.3 minutes to complete the 50% compression with a strain rate of 0.001 s^{-1}. In other words, deformed conditions have experienced an expressively higher diffusional activity than heat-treated conditions at 700°C and 900°C.

In fact, EDS analyses carried out within α grains and laths in the three conditions have yielded the Al contents presented in **Table 3**, which show that the α phase is richer in Al in the Ti64_700C_D condition and leaner in the Ti64_900C_HT condition. These results are also helpful to understand the precipitation of secondary α in the β phase in the Ti64_900C_HT condition against the absence of such precipitation in Ti64_700C_D, as previously discussed. In the latter, the α phase is richer in α-stabilizing elements, thus making β lean in these elements and hindering secondary α precipitation in these conditions. Furthermore, oxygen is known to promote the precipitation of Ti_3Al phase by decreasing the solubility of Al in the α phase [34]. In a study of Ti-64 alloy with 0.07 and 0.19 wt% O, Welsch and Bunk have observed the presence of α_2 after aging at 550°C for 115 h only in the alloy with the highest oxygen content [35]. Lim et al. have found that the increase of oxygen content in a Ti-8 wt% Al alloy not only increases the volume fraction of α_2 after aging, but also changes its distribution from heterogeneous (concentrated at dislocations) to uniform. In their work, the phase has precipitated even with oxygen concentrations as low as 580 ppm (0.058 wt%) after aging at 695°C during 200 h [36], which reinforces the cooperative effect of Al and O concentrations and aging temperature on the precipitation of this phase. However, so far, no systematic correlation between the $\alpha + \alpha_2$ *solvus* line and the oxygen content has been established. Overall, studies focused on Ti-64 alloy with oxygen concentrations up to 0.22 wt% have observed the formation of Ti_3Al [14,26,35]. Therefore, the amount of oxygen in the present alloy, 0.14 wt%, is enough to aid the formation of the intermetallic phase. In the present work, EDS results have shown that the β phase contains no detectable amount of oxygen and therefore one can assume that this element partitions in its totality to the α phase.

Condition	Ti64_700C_D	Ti64_900C_D (α_P)	Ti64_900C_D (α_S)	Ti64_900C_HT
Al content (wt%)	7.3 ± 0.1	6.2 ± 0.1	3.8 ± 0.3	5.2 ± 0.4

Table 3. Al contents of the α phase in different conditions of the Ti-64 alloy.

4.3. Early stages of aging treatment

Shorter aging treatments with soaking time of 8 h were carried out in situ to enable the tracking of the alloy's behavior with its different initial microstructures in the early stages of aging. **Fig. 9** shows the behavior of the α/α' phase in conditions where martensite was majorly present in the initial microstructure. In X-ray diffraction, peak broadening might be a result of chemical inhomogeneity and lattice distortions, and lattice parameters are also sensitive to chemical composition [37,38]. Because α' is a supersaturated substitutional phase [6], it can be assumed that its reflections present themselves broader than the reflections of the chemically stable α phase. Furthermore, its consequently strained state also contribute to the broadening of their reflections [31]. Taking this into account, the full width at half maximum (FWHM) of $(10\bar{1}1)\alpha$, the most intense reflection of the α phase, was calculated ($R^2 \geq 0.9892$), and results are shown in **Fig. 9a**, while **Fig. 9b** presents the evolution of the lattice parameters of α/α', obtained via Rietveld refinement (Rwp ≤ 0.1194 and standard error ≤ 9.32×10^{-4} Å), in the form of the c/a aspect ratio.

In all conditions, a decrease in the FWHM values is seen. The lower initial FWHM value of Ti64_700C_HT indicated that this condition presents a lower degree of chemical inhomogeneity and internal strain, which is in agreement with its lamellar/martensitic microstructure. The decrease is more accentuated within the first hour of aging and in the remaining time this parameter tends to stabilize. This implies that, in all these systems, the α' phase undergoes chemical and lattice homogenization and such homogenization is intensified in the beginning of the treatment. Results are in good agreement with previous studies on the martensite decomposition in Ti-64 alloys tracked by the increase in hardness values [9,10].

Regarding the ratio between the lengths of *c* and *a* parameters of the hexagonal lattice, it is noticeable that Ti64_1050C_HT and Ti64_1050C_D follow the same tendency, with the increase of the c/a ratio during aging, while Ti64_700C_HT follows the opposite tendency, i.e. its c/a ratio decreases during the isothermal treatment. Both *a* and *c* parameters decrease in length; however, the percent decrease of the a-axis is larger than the decrease of the c-axis for Ti64_1050C_D and Ti64_1050C_HT, whereas the decrease of c-axis is larger in Ti64_700C_HT. The variation of lattice parameters is a direct consequence of the diffusion of interstitial and substitutional atoms; since martensite, in this case, is a supersaturated substitutional solution, the variation is mostly affected by the diffusion of substitutional atoms. The increase in c/a ratio is known to harden and strengthen the alloy due to the restriction in the number of activated slip systems in the hexagonal structure [35,39]. Thus, this is a plausible explanation

for the hardening of the alloy upon conversion of the α' phase into α. Regarding Ti64_700C_HT, the reduction in the c/a ratio might be related the early presence of the stable α phase, in contrast with the martensitic microstructure present in both conditions produced at 1050°C, which results in different chemical distributions between α and α' phases and between the α/α' set and β. Because no deconvolution between α and α' peaks is possible, their behavior comes as a sum of the behavior of each component alone.

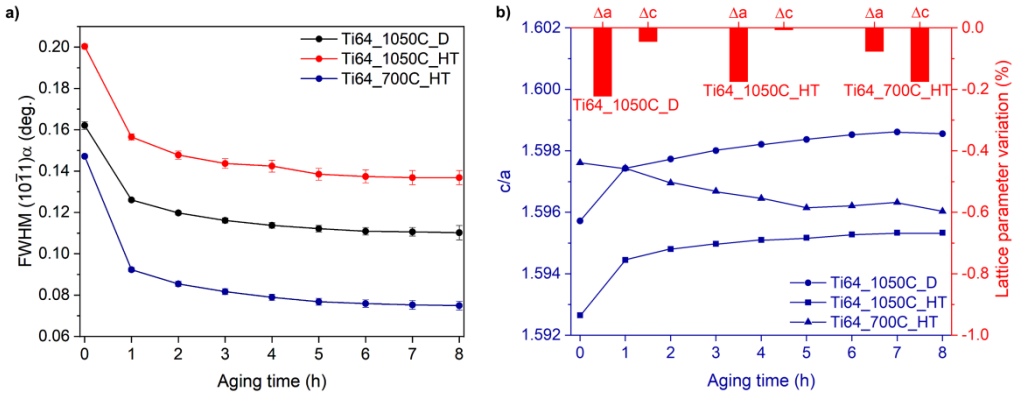

Fig. 9. a) (**10$\bar{1}$1**) FWHM and **b)** lattice parameters evolution of the α/α' phase during aging of Ti64_1050C_D, Ti64_1050C_HT and Ti64_700C_HT conditions.

Fig. 10 depicts the behavior of the β phase during the first eight hours of aging in conditions where the phase was present with a higher fraction, namely Ti64_900C_HT, Ti64_900C_D and Ti64_700C_D. Such behavior is exemplified by the main β reflection, (110). In all cases, a decrease in the cell length of β, which causes an increase in the 2theta position of the reflections of the phase, is seen. This decrease is more easily seen in the Ti64_700C_D condition. Such behavior can be explained by the partitioning of solute, most specifically V, in the β phase. Elmer et al. [40] have observed a decrease in the lattice parameter of β at temperatures near 500°C, and Barriobero-Vila et al. [41] have observed the same behavior of the β phase in a Ti-6Al-6V-2Sn alloy also at temperatures close to the one used in this work. They have attributed this behavior to the enrichment of V in the β phase with a simultaneous depletion of Ti by this phase, basically driven by an attempt of the system to reach thermodynamic equilibrium. In this regard, the contraction owes itself to the smaller atomic radius of V, and also of Fe, in comparison to that of Ti. Elmer et al. further proposes that the decrease in the lattice parameter of β can be a consequence of the relaxation of internal stresses created by the different lattice expansion rates of α and β phases during heating [40].

In Ti64_900C_HT condition, a sharp increase in intensity and decrease in width can be noticed. ThermoCalc® simulations described in **Section 2.4** show that the equilibrium weight fraction of the β

phase at 900°C is of approximately 62%, against 5.5 wt% at 700°C. The volume fraction shown in **Table 2**, equivalent to a weight fraction of ~10%, deviates significantly from this value. This indicates that the thermal/thermomechanical treatments imposed to the alloy in these conditions, in addition to the rapid cooling to room temperature, induce the formation of a metastable system. Thus, the behavior of the β phase might be, again, a consequence of an attempt to achieve equilibrium in the beginning of the subsequent isothermal treatment. The absence of this behavior in the Ti64_900C_D might be explained by the fact that the β phase remaining after deformation transforms almost completely into secondary α colonies, as can be seen in **Fig. 2**. In this case, the final β phase is enriched in β-stabilizing elements due to depletion from the secondary α phase in comparison with the isolated β islands between primary α lamellae seen in Ti64_900C_HT condition [42].

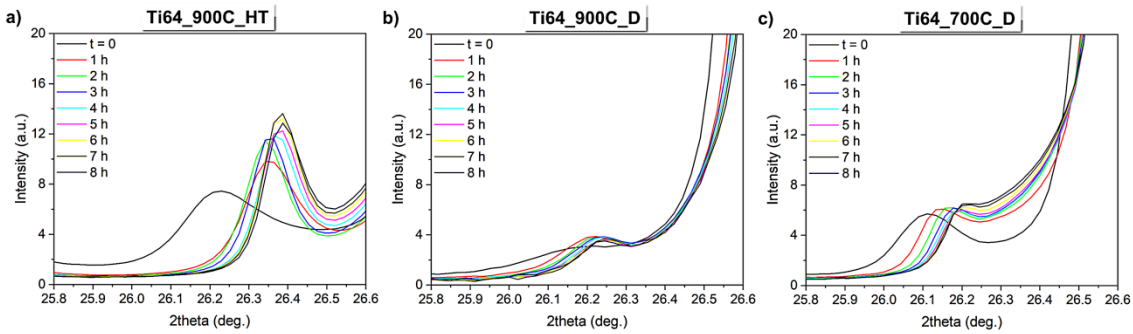

Fig. 10. Behavior of the (110)β reflection during aging of **a)** Ti64_900C_HT, **b)** Ti64_900C_D and **c)** Ti64_700C_D conditions.

5. Conclusions

The response of Ti-6Al-4V alloy with different starting microstructures to aging treatment has been evaluated. From this study, the following conclusions can be drawn:

- A wide variety of microstructures, ranging from martensitic to globular morphologies of the α phase with different amounts of the β phase, can be achieved by an adequate selection of thermal and thermomechanical processing routes.
- All produced microstructures have shown some degree of hardening after aging at 500°C/24h. The conditions with the highest hardness values after aging were those with a predominantly martensitic microstructure, but the best response to aging in terms of hardness increase was shown in conditions with globular, Widmanstätten and bimodal microstructures with a higher content of β phase.
- In conditions with martensitic microstructure, the main contribution to the hardening of the alloy arises from the transformation of the martensitic α' phase into α, whereas in conditions with a high amount of β phase, hardening takes place by the decomposition of this phase into fine α platelets,

and the precipitation of Ti_3Al also contributes to hardening when a high amount of primary α sufficiently enriched in Al and O is present.

- The distribution of the remaining β phase influences the precipitation of secondary α during aging, favoring such precipitation when it presents itself continuous along the boundaries of the α phase and hindering the precipitation when it is discontinuous and concentrated in triple boundaries.
- In situ analysis of the early stages of aging treatments show that the decomposition of the metastable α' phase is intensified in the beginning of the treatment. The reduction of the FWHM of reflections indicates homogenization by the conversion into the stable α phase and the increase of the c/a ratio indicates a contribution to hardening by the reduction in the number of active slip systems.
- In situ analysis of the early stages of aging treatments also show that the β undergoes chemical homogenization and shrinkage, which is caused by the difference in atomic radii of the partitioning elements.

Acknowledgements

The Materials Department of the Federal University of São Carlos (DEMa – UFSCar, São Carlos, Brazil) and the Metals Characterization and Processing Laboratory of the Brazilian Center for Research in Energy and Materials (CNPEM, Campinas, Brazil) are acknowledged for granting access to their facilities for the conduction of thermal and thermomechanical treatments and for TEM and EBSD analyses. The Deutsches Elektronen Synchrotron (Hamburg, Germany) is acknowledged for the use of P07B beamline and the Brazilian Synchrotron Light Laboratory is acknowledged for the use of XTMS experimental station of the XRD1 beamline for the (HE)XRD experiments hereby presented.

Funding

This work was supported by the National Council for Scientific and Technological Development – CNPq (grant number 161959/2015-6), by the Coordination for the Improvement of Higher Education Personnel – CAPES (grant number 88887.302880/2018-00 and PROBRAL project 88881.143948/2017-01), by the German Academic Exchange Service – DAAD (project DAAD PPP-Brazil 2018 – ID 57390937), by Fundação para a Ciência e Tecnologia (FCT – MCTES) via the project UIDB/00667/2020 (UNIDEMI) and by the CALIPSOplus project under the Grant Agreement 730872 from the EU Framework Programme for Research and Innovation HORIZON 2020 (project reference I-20190492 EC). H. C. Pinto is CNPq fellow. The funding source had no involvement in the development of the research or in the preparation of the article.

Declaration of interest

No conflicts of interest exist.

Data availability

The raw/processed data required to reproduce these findings cannot be shared at this time due to technical or time limitations.

References

[1] I. Polmear, D. StJohn, J.-F. Nie, M. Qian, Light alloys: Metallurgy of the light metals, 5th ed., Elsevier, 2017.

[2] C. Leyens, M. Peters, eds., Titanium and titanium alloys, Wiley-VCH, 2003.

[3] G. Lütjering, J.C. Williams, Titanium, 2nd ed., Springer, 2007.

[4] F.H. Froes, ed., Titanium: Physical metallurgy, processing and applications, ASM International, 2015.

[5] M.J. Donachie Jr., Titanium: a technical guide, 2nd ed., ASM International, 2000.

[6] M. Motyka, A. Baran-Sadleja, J. Sieniawski, M. Wierzbinska, K. Gancarczyk, Decomposition of deformed α′(α″) martensitic phase in Ti-6Al-4V alloy, Mater. Sci. Technol. (United Kingdom). 35 (2019) 260–272. doi:10.1080/02670836.2018.1466418.

[7] T. Morita, K. Hatsuoka, T. Iizuka, K. Kawasaki, Strengthening of Ti-6Al-4V alloy by short-time duplex heat treatment, Mater. Trans. 46 (2005) 1681–1686. doi:10.2320/matertrans.46.1681.

[8] M. Stephen, M. Kalenda, S. Charles, S. Waldo, Effect of ageing treatment on the microstructure and hardness of the Ti6Al4V alloy, Mater. Sci. Forum. 829 (2015) 194–199. doi:10.4028/www.scientific.net/MSF.828-829.194.

[9] J.I. Qazi, O.N. Senkov, J. Rahim, F.H. Froes, Kinetics of martensite decomposition in Ti-6Al-4V-xH alloys, Mater. Sci. Eng. A. 359 (2003) 137–149. doi:10.1016/S0921-5093(03)00350-2.

[10] F.X. Gil Mur, D. Rodríguez, J.A. Planell, Influence of tempering temperature and time on the α'-Ti-6Al-4V martensite, J. Alloys Compd. 234 (1996) 287–289. doi:10.1016/0925-8388(95)02057-8.

[11] R. Pederson, Microstructure and phase transformation of Ti-6Al-4V, Luleå University of Technology, 2002.

[12] B.D. Venkatesh, D.L. Chen, S.D. Bhole, Effect of heat treatment on mechanical properties of

Ti-6Al-4V ELI alloy, Mater. Sci. Eng. A. 506 (2009) 117–124. doi:10.1016/j.msea.2008.11.018.

[13] S. Hémery, P. Villechaise, On the influence of ageing on the onset of plastic slip in Ti-6Al-4V at room temperature: Insight on dwell fatigue behavior, Scr. Mater. 130 (2017) 157–160. doi:10.1016/j.scriptamat.2016.11.042.

[14] Z. Wu, C. Qiu, V. Venkatesh, H.L. Fraser, R.E.A. Williams, G.B. Viswanathan, M. Thomas, S. Nag, R. Banerjee, M.H. Loretto, The influence of precipitation of alpha2 on properties and microstructure in TIMETAL 6-4, Metall. Mater. Trans. A. 44 (2013) 1706–1713. doi:10.1007/s11661-012-1530-9.

[15] H. Carreon, A. Ruiz, B. Santoveña, Study of aging effects in a Ti-6Al-4V alloy with Widmanstätten and equiaxed microstructures by non-destructive means, in: AIP Conf. Proc., 2014: pp. 739–745. doi:10.1063/1.4864894.

[16] S. El-Hadad, M. Nady, W. Khalifa, A. Shash, Influence of heat treatment conditions on the mechanical properties of Ti-6Al-4V alloy, Can. Metall. Q. 57 (2018) 186–193. doi:10.1080/00084433.2017.1412557.

[17] Y. Ji, T.W. Heo, F. Zhang, L.Q. Chen, Theoretical assessment on the phase transformation kinetic pathways of multi-component Ti alloys: Application to Ti-6Al-4V, J. Phase Equilibria Diffus. 37 (2016) 53–64. doi:10.1007/s11669-015-0436-9.

[18] I. Ansara, T. Dinsdale, M.H. Rand, COST 507 - Thermomechanical database for light metal alloys, 1998.

[19] F. Zhang, S. Chen, Y.A. Chang, N. Ma, Y. Wang, Development of thermodynamic description of a pseudo-ternary system for multicomponent Ti64 alloy, J. Phase Equilibria Diffus. 28 (2007) 115–120. doi:10.1007/s11669-006-9006-5.

[20] L.G. Martinez, R.U. Ichikawa, K. Imakuma, M.T.D. Orlando, X. Turrillas, Synchrotron diffraction characterization of alternative powder diffraction standards, An. Do V Encontro Científico Física Apl. (2014) 115–117. doi:10.5151/phypro-ecfa-051.

[21] L. Lutterotti, S. Matthies, H.-R. Wenk, A.S. Schultz, J.W. Richardson, Combined texture and structure analysis of deformed limestone from time-of-flight neutron diffraction spectra, J. Appl. Phys. 81 (1997) 594. doi:10.1063/1.364220.

[22] X.F. Gu, T. Furuhara, W.Z. Zhang, PTCLab: free and open-source software for calculating phase transformation crystallography, J. Appl. Crystallogr. 49 (2016) 1099–1106. doi:10.1107/S1600576716006075.

[23] L. Guo, X. Fan, G. Yu, H. Yang, Microstructure control techniques in primary hot working of

titanium alloy bars: A review, Chinese J. Aeronaut. 29 (2015) 30–40. doi:10.1016/j.cja.2015.07.011.

[24] A. Gheysarian, M. Abbasi, The effect of aging on microstructure, formability and springback of Ti-6Al-4V titanium alloy, J. Mater. Eng. Perform. 26 (2017) 374–382. doi:10.1007/s11665-016-2431-7.

[25] K. Sofinowski, M. Šmíd, I. Kuběna, S. Vivès, N. Casati, S. Godet, H. Van Swygenhoven, In situ characterization of a high work hardening Ti-6Al-4V prepared by electron beam melting, Acta Mater. 179 (2019) 224–236. doi:10.1016/j.actamat.2019.08.037.

[26] A. Radecka, P.A.J. Bagot, T.L. Martin, J. Coakley, V.A. Vorontsov, M.P. Moody, H. Ishii, D. Rugg, D. Dye, The formation of ordered clusters in Ti-7Al and Ti-6Al-4V, Acta Mater. 112 (2016) 141–149. doi:10.1016/j.actamat.2016.03.080.

[27] J.C. Williams, R.G. Baggerly, N.E. Paton, Deformation behavior of HCP Ti-Al alloy single crystals, Metall. Mater. Trans. A. 33 (2002) 837–850. doi:10.1007/s11661-002-1016-2.

[28] M.J. Blackburn, The ordering transformation in titanium: aluminium alloys containing up to 25 at. pct. Al, Trans. Metall. Soc. AIME. 239 (1967) 1200–1208.

[29] T.K.G. Namboodhiri, C.J. McMahon Jr., H. Herman, Decomposition of the α-phase in titanium-rich Ti-Al alloys, Metall. Trans. 4 (1973) 1323–1331. doi:10.1007/BF02644528.

[30] H. Wu, G. Fan, L. Geng, X. Cui, M. Huang, Nanoscale origins of the oriented precipitation of Ti3Al in Ti-Al systems, Scr. Mater. 125 (2016) 34–38. doi:10.1016/j.scriptamat.2016.07.037.

[31] P. Barriobero-Vila, J. Gussone, J. Haubrich, S. Sandlöbes, J. Da Silva, P. Cloetens, N. Schell, G. Requena, Inducing stable α + β microstructures during selective laser melting of Ti-6Al-4V using intensified intrinsic heat treatments, Materials (Basel). 10 (2017) 1–14. doi:10.3390/ma10030268.

[32] A. Radecka, J. Coakley, V.A. Vorontsov, T.L. Martin, P.A.J. Bagot, M.P. Moody, D. Rugg, D. Dye, Precipitation of the ordered α2 phase in a near-α titanium alloy, Scr. Mater. 117 (2016) 81–85. doi:10.1016/j.scriptamat.2016.02.015.

[33] S.L. Semiatin, N.C. Levkulich, C.A. Heck, A.E. Mann, N. Bozzolo, A.L. Pilchak, J.S. Tiley, Transient plastic flow and phase dissolution during hot compression of α/β titanium alloys, Metall. Mater. Trans. A. (2020). doi:10.1007/s11661-020-05673-9.

[34] R. Boyer, G. Elsch, E.W. Collins, Materials property handbook: titanium alloys, ASM International, 1994.

[35] G. Welsch, W. Bunk, Deformation modes of the α-phase of Ti-6Al-4V as a function of oxygen concentration and aging temperature, Metall. Trans. A. 13 (1982) 889–899. doi:10.1007/

BF02642403.

[36] J.Y. Lim, C.J. McMahon, D.P. Pope, J.C. Williams, The effect of oxygen on the structure and mechanical behavior of Aged Ti-8 Wt pct Al, Metall. Trans. A. 7 (1976) 139–144. doi:10.1007/BF02644050.

[37] E. Aeby-Gautier, F. Bruneseaux, J. Da Costa Teixeira, B. Appolaire, G. Geandier, S. Denis, Microstructural formation in Ti alloys: In-situ characterization of phase transformation kinetics, JOM. 59 (2007) 54–58. doi:10.1007/s11837-007-0011-x.

[38] T. Ungár, Microstructural parameters from X-ray diffraction peak broadening, Scr. Mater. 51 (2004) 777–781. doi:10.1016/j.scriptamat.2004.05.007.

[39] J.M. Oh, B.G. Lee, S.W. Cho, S.W. Lee, G.S. Choi, J.W. Lim, Oxygen effects on the mechanical properties and lattice strain of Ti and Ti-6Al-4V, Met. Mater. Int. 17 (2011) 733–736. doi:10.1007/s12540-011-1006-2.

[40] J.W. Elmer, T.A. Palmer, S.S. Babu, E.D. Specht, In situ observations of lattice expansion and transformation rates of α and β phases in Ti-6Al-4V, Mater. Sci. Eng. A. 391 (2005) 104–113. doi:10.1016/j.msea.2004.08.084.

[41] P. Barriobero-Vila, G. Requena, T. Buslaps, M. Alfeld, U. Boesenberg, Role of element partitioning on the α-β phase transformation kinetics of a bi-modal Ti-6Al-6V-2Sn alloy during continuous heating, J. Alloys Compd. 626 (2015) 330–339. doi:10.1016/j.jallcom.2014.11.176.

[42] G. Geandier, E. Aeby-Gautier, A. Settefrati, M. Dehmas, B. Appolaire, Study of diffusive transformations by high energy X-ray diffraction, Comptes Rendus Phys. 13 (2012) 257–267. doi:10.1016/j.crhy.2011.12.001.